Materials and Design 54 (2014) 236–244

Contents lists available at ScienceDirect

Materials and Design

journal homepage: www.elsevier.com/locate/matdes

Joining of metal to plastic using friction lap welding

F.C. Liu [a], J. Liao [b], K. Nakata [a,*]

[a] JWRI, Osaka University, 11-1 Mihigaoka Ibaraki, Osaka 567-0047, Japan
[b] Kurimoto Ltd, 2-8-45 Suminoe, Osaka 559-0021, Japan

ARTICLE INFO

Article history:
Received 4 June 2013
Accepted 16 August 2013
Available online 24 August 2013

Keywords:
Friction lap welding
Joining
Aluminium
Nylon
Cohesive fracture
Friction stir welding

ABSTRACT

Friction lap welding (FLW) is a new conception of joining method developed in Joining and Welding Research Institute (JWRI). The efficiency of joining metal and plastic using FLW was demonstrated through a case study on aluminium alloy AA6061 and MC Nylon-6. The lap joints with high shear strength were obtained over a wide range of welding parameters. A linear relationship was observed between FLW parameters $(R/v)^{0.5}$ and the thickness of melted nylon (H). The influences of FLW parameters on bubbles and shear strength were investigated. The morphologies of the fractured surfaces of AA6061 alloy fell into seven types based on the scanning electron microscopy examination. Statistical analysis showed that the contribution to shear strength of these regions followed such an order: region II > region V > region VI > region VII > region IV > region I or III.

1. Introduction

Plastics-based materials have been widely and are expected to be more extensively used in automobile, aerospace, and electronic industries due to their low weight, considerable strength, excellent corrosion resistance, thermal and electrical insulation, and design flexibility [1,2]. This has led to high demands on and research interesting in joining dissimilar materials involving plastics and metallic materials for structural applications. Such joining enables engineers to utilize the hybrid components in sections where high stiffness and strength can be exploited, and plastic material offers excellent functional integration.

Joining a metal and a plastic is often difficult and the combined behaviours are grossly not fully understood. This is because of the difference in mechanical and physical properties between the metal and plastic materials, and the limited joining methods available for this type of hybrid materials [3]. Mechanical fastening and adhesive bonding are commonly applied in joining between polymer and metal. These approaches are usually associated with some drawbacks such as long processing time, accidental disassembly, and susceptibility to degradation by environmental factors [4,5]. In order to solve these problems, several welding methods, such as laser joining, ultrasonic welding and friction spot joining have been investigated to exploit the possibility of obtaining high quality hybrid joints of plastics and metals.

Recently, Katayama et al. have developed a laser direct joining process for metals and plastics [1,5,6]. In this process, metal and plastic were part overlapped initially, and then laser beam was irradiated on the overlapped region. The metal was heated up by the moving laser beam, resulting in that the plastic in a narrow region adjacent the heated metal was melted and re-solidified during the laser joining process. The metal and plastic were bonded together during this process. This technique has been proved to have the potentials in producing high performance joints between plastics and various kinds of metallic materials [1,5–10]. The limitation of this process is that there are too many welding parameters, such as laser power, welding speed, pulse mode, focus shape and size, beam quality, polarization and keyhole shielding gas which can influence the quality and reliability of the eventual joint.

In the past few years, Balle et al. [11–13] have investigated ultrasonic lap welding of aluminium alloys and fibre reinforced polymers. The tensile shear strength of these joints reached up to about 21–24 MPa and typical cohesive failures were observed on the fracture surface of aluminium alloys [11,12]. The welding time for ultrasonic welding was a few seconds which made the process ideal for mass production. It should however be noted that this joining technique is limited to small components with weld lengths typically not exceeding a few centimetres.

Some newly raised research works have demonstrated that friction spot joining (FSJ) also is an alternative joining technology for plastic-metal hybrid joints [14,15]. The plastic-metal joints obtained by FSJ exhibited a higher joint strength as compared to adhesive joining [14]. The main advantages of this technique include: short joining cycles, absence of emissions, operation simplicity, available of commercial equipment and good mechanical performance [14]. Only overlap configurations and spot geometry joint design limit its application.

* Corresponding author. Tel./fax: +81 0668798656.
E-mail address: nakata@jwri.osaka-u.ac.jp (K. Nakata).

0261-3069/$ - see front matter © 2013 Elsevier Ltd. All rights reserved.
http://dx.doi.org/10.1016/j.matdes.2013.08.056

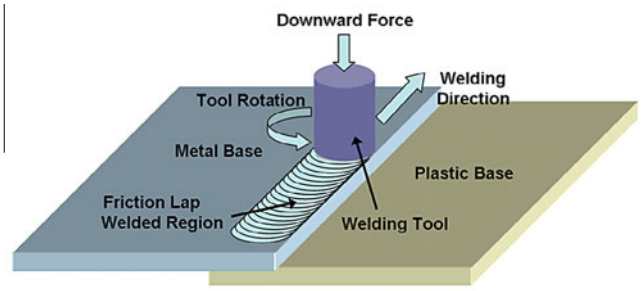

Fig. 1. Schematic illustration of joining metal and plastic through FLW.

Table 2
Mechanical and physical properties of AA6061-T6 and MC Nylon-6.

	AA6061-T6	MC Nylon-6
Ultimate tensile stress (MPa)	318	81
Yield stress (MPa)	289	–
Modulus of elasticity (GPa)	68.9	2.79
Elongation at break (%)	11	26
Density (g cm^{-3})	2.70	1.15
Melting temperature (°C)	582–652	216
Glass transition temperature (°C)	–	50
Thermal conductivity (W m^{-1} K^{-1})	167	0.25
Coefficient of thermal expansion, linear 20 °C (μm m^{-1} K^{-1})	23.6	90
Specific heat capacity (J g^{-1} K^{-1})	0.90	1.65

All these emerging technologies for joining metals and plastics have their own advantages alongside of disadvantages. New joining techniques for metal and polymer hybrid joints which offer better joint properties and increased design flexibility compared to existing techniques are highly required.

In this study, the authors firstly showed the feasibility of joining metal to plastic using friction lap welding (FLW) through a case study on two commercially available materials, aluminium alloy AA6061 and MC Nylon-6. In addition to the joint interfaces, the fractography of the tensile specimens and the factors which influence the quality of the FLW hybrid joints have been investigated.

2. Friction lap welding

Friction lap welding which is developed in JWRI, Osaka University [16] is a new conception of joining method for metal–plastic hybrid joints. As shown in Fig. 1, a non-consumable rotation tool is pressed on the surface of metal matrix and travels long the overlap region. The appearance of the FLW process is similar to the friction stir welding (FSW) [17,18]. The main difference between the FLW and FSW is that the FLW tool does not have a stir pin, and therefore, the primary function of the rotation tool is not to cause materials flow around the stir pin but to press and heat up the metal workpiece. The localized heating is accomplished by friction between the tool shoulder and the metal workpiece. The heat transfers via conduction from the heated metal component to the plastic component and consequently melts the plastic materials in a narrow region adjacent to the interface. Bonding between the metal and the plastic can be finished after the melted plastic is solidified under the pressure provided by the pressed metal component.

3. Materials and experimental procedures

Aluminium alloy (A6061) and monomer casting nylon (MC Nylon-6) sheets with dimensions of 150 × 75 × 2 mm were prepared. The chemical composition of the AA6061 is listed in Table 1. The MC Nylon-6 was prepared by the alkali-catalyzed anionic ring-opening polymerization of caprolactam. Compared with normal Nylon-6, MC Nylon-6 has the advantages of a simple preparation procedure, high crystallinity, high molecular weight and excellent properties. The physical properties of the AA6061 and the MC Nylon-6 are compared in Table 2. FLW processes were conducted using a FSW machine with a specially designed cylindrical tool. The diameter of the tools used in this study was 15 and 20 mm, respectively. During FLW, a position control system was employed, and the plunging depth was set to 0.3 mm. The cylindrical tool remained perpendicular to the workpiece surface during FLW. The rotation rate (R) was varied from 1000 to 3000 rpm and the welding speed (v) was varied from 200 to 1500 mm/min. The FLW samples were designated using a series digital format. For example, sample 1000–200 denotes the sample which was subjected to FLW at a rotation rate of 1000 rpm and a welding speed of 200 mm/min.

After welding, the FLW samples were cut into strips perpendicular to the welding direction for joint interface examinations and tensile shear test. The width of the strips is about 20 mm. The cross sections for joint interface examinations were mechanically ground and polished with 1 μm diamond past. The thickness of re-solidified layer and non-melted layer of nylon plates was measured at the middle of the weld zone. Tensile shear test was carried out using a tensile test machine (SHIMAZU) at a tensile speed of 0.5 mm/min. The grip inserts were used so that the centreline of the grip assembly is aligned with the bonded interface. The fracture surfaces of the tensile samples were subjected to optical microscopy (OM), scanning electron microscopy (SEM) and SEM–EDS (energy dispersive X-ray spectrometer) analyses.

4. Results and discussion

4.1. Joint produced using a 20 mm diameter tool

A cylindrical tool with dimension of 20 mm in diameter and an overlap of 22 mm were initially used to join the AA6061 plate to the MC Nylon-6 plate. The selected processing parameters were: a rotation rate of 2000 rpm, a traverse speed of 600 mm/min and a plunge depth of 0.3 mm. Fig. 2 shows the typical joint samples processed by FLW before and after tensile test. The semi-circular patterns which were generally observed in the friction stir welded/processed samples [19] were clearly observed on the surface of processed AA6061 (Fig. 2a). The FLW sheets did not show apparent welding distortion and warping. This is especially attractive for structural applications in manufacturing industries because the cost and time required for distortion correcting can be saved.

Tensile test showed that the FLW samples did not fail through the weld interface but failed across the nylon sheet near the edge of the weld zone, as shown in Fig. 2c. Such a strong joint was produced by FLW without any treatment on the surface of the AA6061

Table 1
Chemical composition of AA6061-T6 plate (wt.%).

	Al	Mg	Si	Fe	Cu	Cr	Mn	Ti	Zn	Others
AA6061	Balance	1.05	0.63	0.29	0.27	0.17	0.07	0.02	0.01	<0.01

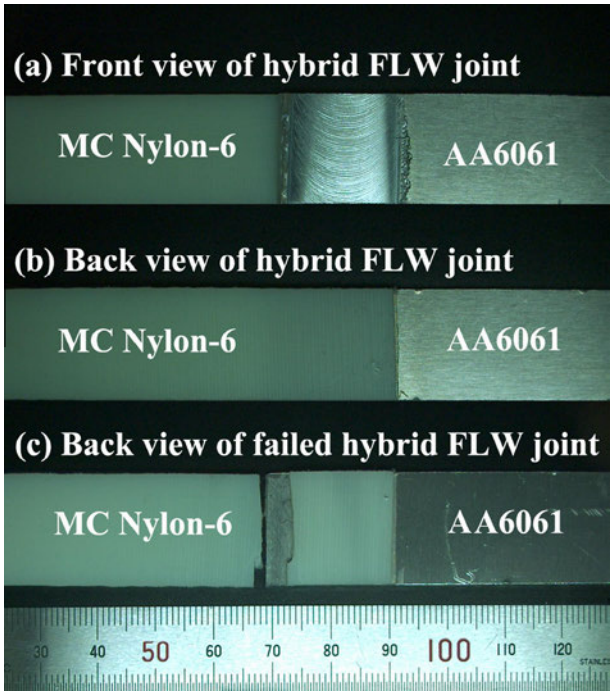

Fig. 2. Typical FLW joint processed using tool with dimension of 20 mm in diameter.

and MC Nylon-6. This demonstrated that FLW is an effective method to obtain sound hybrid joints of metal and plastic.

4.2. Shear strength of hybrid lap joints

In order to evaluate the influence of welding parameters on the tensile shear strength of the metal–plastic hybrid joints, and thereby developing more insights into the FLW of metal and plastic and optimising the welding parameters, a 15 mm diameter tool and an overlap of 17 mm were selected for the purpose of reducing the weld area, so that the FLWed samples may fracture through the weld interface in tensile test. Fig. 3 summarizes the nominal shear strength (NSS) of the joints produced under various parameters. After FLW, the MC Nylon-6 and AA6061 were tightly bonded together in the whole lapped region (Fig. 4). In this case, the NSS was calculated from the maximum load divided by the lapped area (the lapped area of the tensile sample is equal to the width of the tensile sample multiplied by the length of the lapped region). Three important observations can be made from Fig. 3. Firstly, highly bonded plastic-metal hybrid joints with NSS varied from about 5 to 8 MPa were obtained over a wide welding parameter range. Secondly, at the welding speed of 200 mm/min, the NSS increased from 5.0 to 7.8 MPa with increasing the rotation rate from 1000 to 3000 rpm. Thirdly, at the rotation rate of 1000 rpm, the NSS increased from 5.0 to 7.4 MPa with increasing the welding speed from 200 to 400 mm/min initially, and then decreased to 5.4 MPa after further increasing the welding speed to 800 mm/min; however, at rotation rates of 2000 and 3000 rpm, the NSS decreased continually with increasing the welding speed from 200 to 1500 mm/min.

The results above showed that the FLW parameters have a great influence on the NSS. Two tendencies could be found from Fig. 3 although the regularity is not obvious: (i) Increasing the rotation rate is beneficial to obtain high strength hybrid joints of the MC Nylon-6 and AA6061 in a wide range of welding speeds. (ii) It is a challenge to acquire high strength hybrid joints of the MC Nylon-6 and AA6061 at high welding speeds.

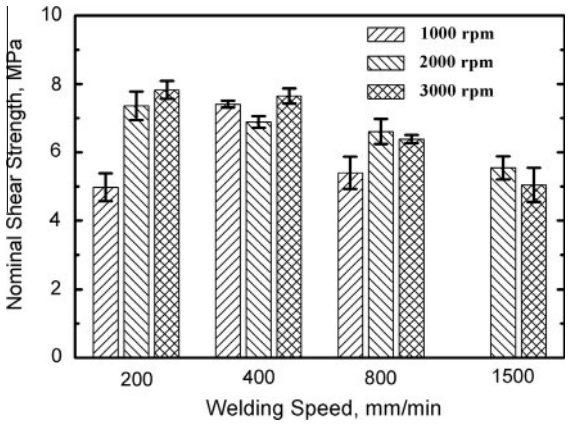

Fig. 3. Nominal shear test results of FLW joints of MC Nylon-6 to AA6061 welded under various parameters.

4.3. Cross-sectional analysis of hybrid lap joints

Fig. 4 exhibits the cross sections of the FLW joints produced under various welding parameters. It is showed that slight deformation occurred on the AA6061 plates. The MC Nylon-6 in a narrow region adjacent to the interface was melted during the FLW process and was re-solidified under the pressure provided by the deformed AA6061 plate pressed by the weld tool after the FLW. The AA6061 and MC Nylon-6 were bonded together during this process. The re-solidified layers in nylon plates could be observed clearly on the cross sections of the FLW joints. It is also clear that the thickness of re-solidified layer highly depended on the welding parameters. A further SEM observation indicated that the bubbles did not contact the AA6061 directly but were separated from the AA6061 by a thin nylon film, as typically shown in Fig. 5a. High magnification observation demonstrated that the MC Nylon-6 and the AA6061 are tightly bonded together (Fig. 5b).

Previous thermogravimetric analysis revealed that the initial decomposition temperature of MC Nylon-6 was 375 °C [20]. Therefore, when the MC Nylon-6 was heated up to temperatures high sufficiently during FLW, the pyrolysis products which mainly consisted of gases such as water vapour, carbon monoxide, carbon dioxide, hydrocarbons and so on were developed. [21], resulting in the bubble formation in the melted MC Nylon-6 in a thin region near the interface, as show in Figs. 4 and 5. It is noted that large sized bubbles were mainly observed in the FLW joints processed at low welding speed (Fig. 4). Bubbles have been extensively observed in laser joining and friction spot joining of plastics and metals [5,6,10,15]. In those processes, the bubbles would generate high pressure points and simultaneously push the molten plastic onto the metal surface, which would result in a tight adherence of the plastic to the metal surface. During FLW, the melted MC Nylon-6 continuously contacted with the AA6061 plate under the pressure of the FLW tool. Therefore, the generation of bubbles is not the essential conditions for joining plastic to metal using FLW.

The ratio of L_b/L_{LR} is summarized in Fig. 6, where L_b is the total length of all the bubbles observed on the cross section of one joint, and L_{LR} is the length of the lapped region of the same joint. It is obvious that the value of L_b/L_{LR} decreased with increasing the welding speed. This phenomenon is easy to be understood. The temperature measurement during FSW showed that the tool shoulder dominated the heat generation [22]. This is attributed to the fact that the contact area and vertical pressure between the tool shoulder and workpiece are much larger than those between the pin and workpiece, and the tool shoulder has a higher linear velocity than the pin with smaller radius [23]. For this reason, the influence of welding parameters on thermal input for

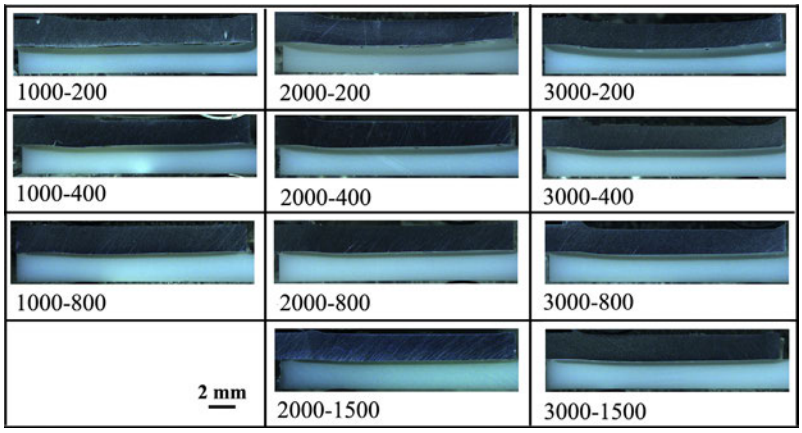

Fig. 4. Cross-sectional macroscope observation for FLW joints of MC Nylon-6 to AA6061 welded under various parameters.

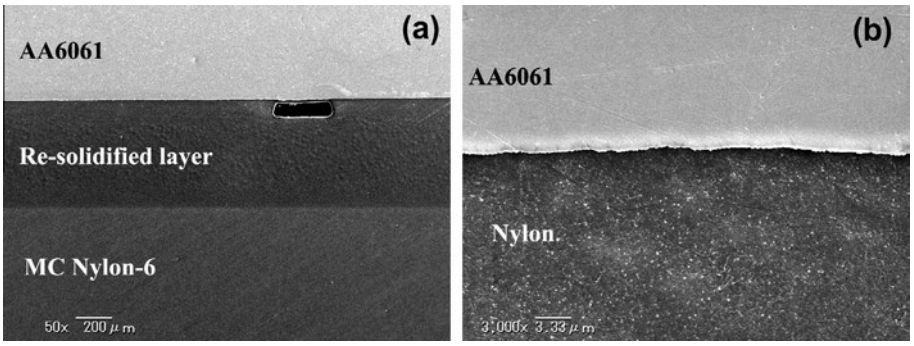

Fig. 5. Cross-sectional SEM observation for FLW joints of MC Nylon-6 to AA6061 welded at 2000 rpm and 400 mm/min.

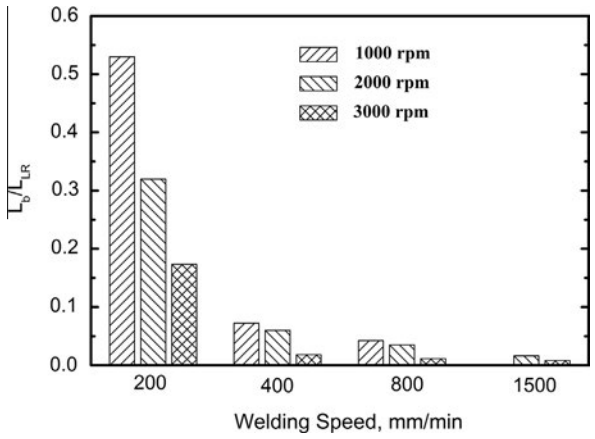

Fig. 6. Variation in L_b/L_{LR} for FLW joints of MC Nylon-6 to AA6061 welded under various parameters.

FLW and FSW is similar. Referring to the FSW studies [18,22,23], an increase in the welding speed reduced both the welding temperature and the high temperature duration during FLW. This was further confirmed by the statistics that the thickness of the re-solidified layers decreased with increasing welding speed at all investigated rotation rates (Fig. 7). The low thermal input at high welding speed reduced the pyrolysis gas generation and bubble formation.

It has been well documented that increasing the FSW rotation rate increased the welding temperature [17,18,22]. However, Fig. 6 shows that the value of L_b/L_L decreased from 0.53 to 0.17 with increasing the rotation rate from 1000 to 3000 rpm at the welding speed of 200 mm/min. This appeared to contradict the foregoing analysis that the high thermal input led to more bubbles during FLW. A further analysis showed that the thickness of nylon plates within the lap joints decreased with increasing the rotation rate (Fig. 7), indicating that part of nylon plates was squeezed out and the amount of the squeezed nylon increased with increasing the rotation rate. It should note that although the FLW was operated under a position control system, the actual descending distance is usually different from the set point because the workpiece stiffness varied with welding temperature. This is a common disadvantage for the existing FSW machines. During FLW, the plastic under the metal sheet was partly melted, and thereafter the metal sheet was bent toward the plastic because

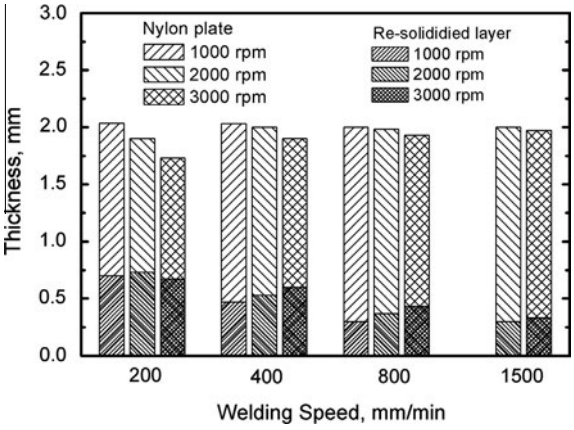

Fig. 7. Variation in thickness of nylon plate and re-solidified layer for FLW joints of MC Nylon-6 to AA6061 welded under various parameters.

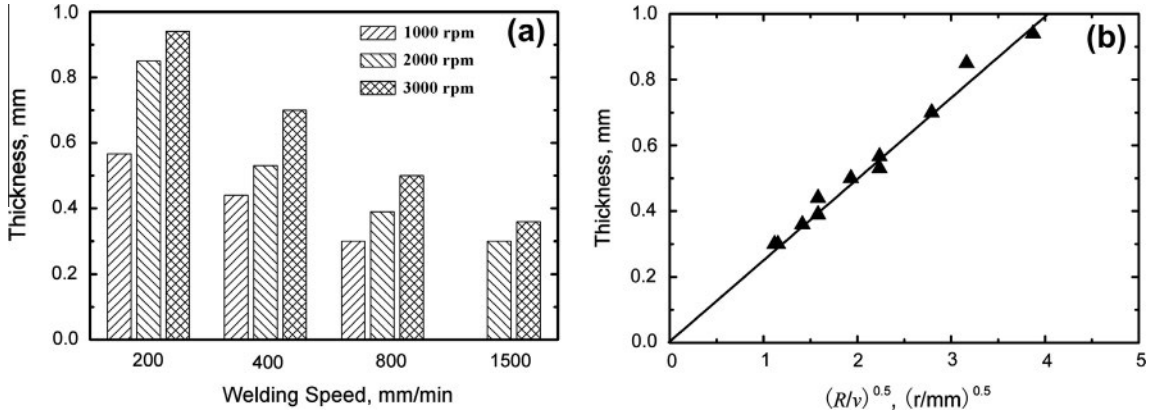

Fig. 8. Variation in thickness of melted nylon with (a) welding speed at various rotation rates and (b) $(R^2/v)^{0.5}$.

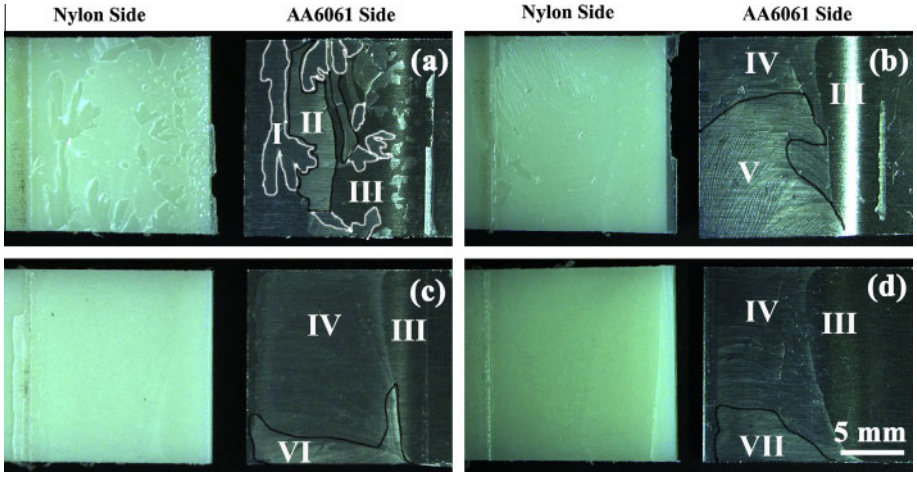

Fig. 9. Fractured surface observation for FLW joints of MC Nylon-6 to AA6061 welded at 2000 rpm and various welding speed: (a) 200 mm/min, (b) 400 mm/min, (c) 800 mm/min and (d) 1500 mm/min.

there is a lack of the supporting force from the plastic to metal sheet. When FLW was processed at high rotation rates, more plastic under the metal sheet was melted and the AA6061 plates were further softened at the higher temperatures. This made the AA6061 plates bent increasingly toward the MC Nylon-6 plates (Fig. 4). Therefore, the increment of the FLW rotation rate not only increases the welding temperature, but also compresses the hybrid joints tightly, which is beneficial to reducing bubbles and enhancing physical or chemical bonding between the AA6061 and MC Nylon-6.

Due to the occurrence of bending deformation in the AA6061 sheet, part of melted nylons was squeezed out. For this reason, the thickness of melted nylon can not be measured directly from the cross sections of the hybrid joints, but should be calculated as the difference between the original thickness of nylon plate and the thickness of nylon which has not been melted. The original thickness of nylon plate was 2 mm. The thickness of nylon which has not been melted could be measured directly from the cross sections of the hybrid joints.

Fig. 8a shows the variation in thickness of melted nylon with welding speed. The thickness of melted nylon increased with increasing rotation rate and decreased with increasing welding speed. This trend is in good agreement with previous investigations that the thermal input during FSW increased with increasing rotation rate and decreased with increasing welding speed [17,22–24].

Arbegast and Hartley [24] proposed a unitized parameter (the pseudo heat index R^2/v) to describe the parameter dependence of the thermal input. They suggested that the general relationship between maximum temperature and FSW parameters for several aluminium alloys can be expressed by

$$\frac{T}{T_m} = K\left(\frac{R^2}{v \times 10^4}\right)^a \tag{1}$$

where T (°C) is the maximum temperature during FSW, T_m (°C) is the melting point of the alloy, the constant K is between 0.65 and 0.75, the exponent v is ranged from 0.04 to 0.06. R (rpm) is the rotation rate, and v (mm/min) is the welding speed. Ren et al. [25] showed that both heat index, R^2/v and R/v , can not be used as the parameters to precisely describe the thermal input, tensile properties and fracture behaviours of FSW 6061Al-T651.

Fig. 8b shows the relationship between the thickness of melted nylon (H) and FLW parameters. All the data fit onto a single straight line which can be expressed by

$$H = A\left(\frac{R}{v}\right)^{0.5} \tag{2}$$

where A is 0.25 in this study. The value of A depends on the tool size and the plunge depth. This indicates that the heat index, (R^2/v), is a valid parameter to predict the thermal input during FLW.

4.4. Fracture morphology of hybrid lap joints

Fig. 9 shows the optical images of the fracture surfaces of the hybrid joints produced by FLW at 2000 rpm and various welding speeds. Residual nylon was observed on the fracture surfaces of all the AA6061 plates. SEM observation demonstrated that the morphology of the fracture surface of AA6061 plates fell into seven types, as typically shown in Fig. 10.

Spherulite morphology (Fig. 10a) was clearly observed in the regions (region I) which were surrounded by white lines in Fig. 9a. Similar spherulites were also observed on the directly opposite MC Nylon-6 surfaces. These demonstrated that the residual nylon in region I was the nylon film attached on the AA6061 plate in the bubble regions (Fig. 5a). SEM observation showed that region II in Fig. 9a was covered by deformed nylon (Fig. 10b), indicating that cohesive fracture took place in the MC Nylon-6 plates. It could be deduced that the nylon in the region II endured some extent of plastic deformation and the region II had a high contribution to the shear strength. In region III (in Fig. 9a), few residual nylon was observed by SEM (Fig. 10c). This is due to that on one hand there is a lack of the interfacial chemical interaction and on the other hand the physical interactions, especially the mechanical interlocking of MC Nylon-6 and AA6061 plate surface, are very weak.

Region IV in Fig. 9b–d exhibited similar morphological characters: the original morphologies of AA6061 surfaces remained observable (Fig. 10d), and high magnification observation showed that thin and small detrital nylon particles were scattered on the AA6061 surface (Fig. 10h). Ridge shaped nylons were detected in regions V, VI and VII on the fracture surfaces of AA6061 (Fig. 10e–g). The morphology of ridge shaped nylons can be regarded as an indicator of the crack propagation paths in the nylon during tensile test. With increasing the welding speed, both the

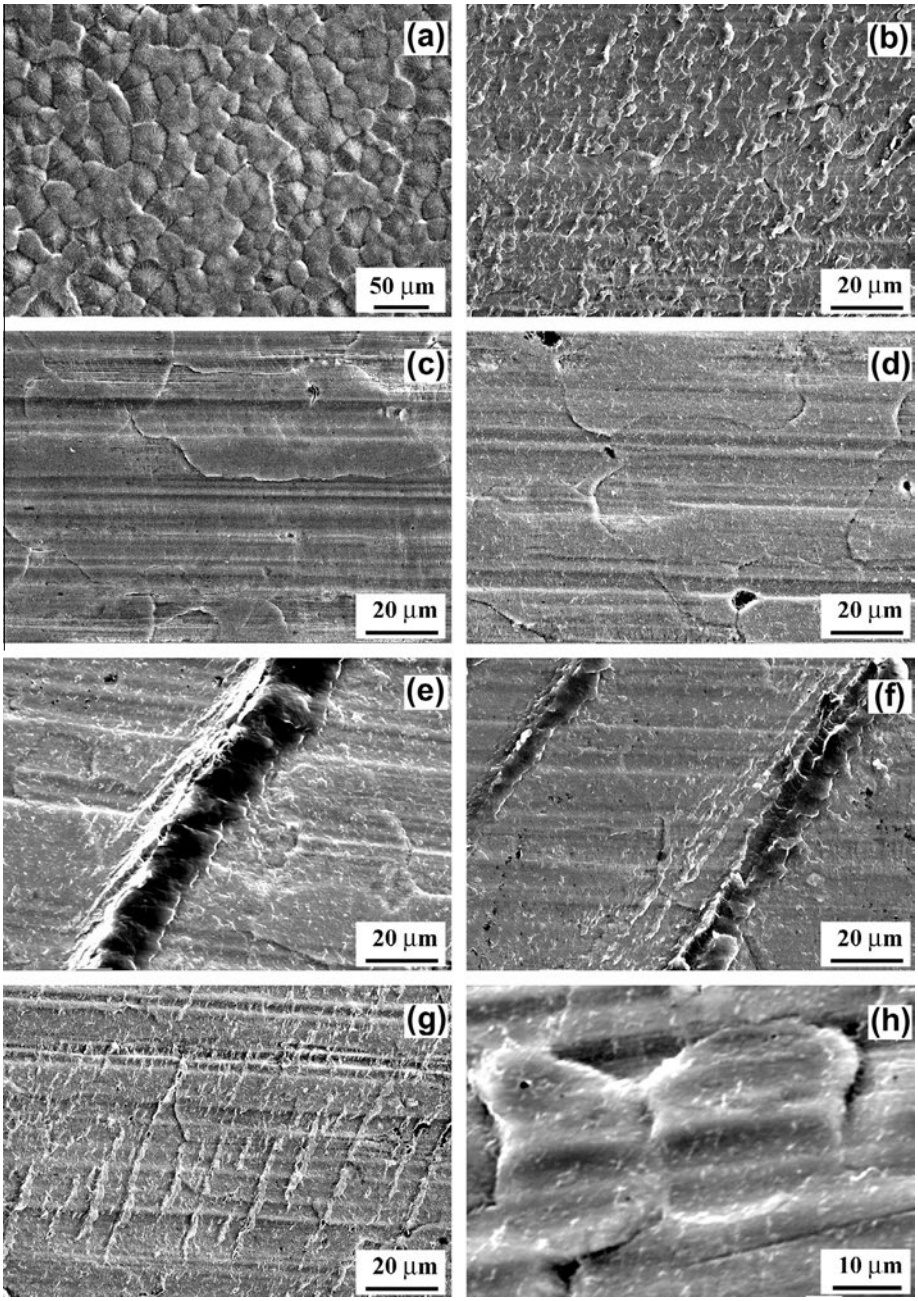

Fig. 10. Typical SEM images obtained from various regions in Fig. 9: (a) region I, (b) region II, (c) region III, (d) region IV, (e) region V, (f) region VI, (g) region VII and (h) high magnification of region IV.

size and distance of the ridge shaped nylons decreased, indicating that the initiation and propagation of cracks in the nylon become easier in these regions.

In order to confirm the distributions of nylon on the fracture surfaces of AA6061, the EDS elemental mappings of C and Al atoms obtained on the fracture surface of Al side were shown in Fig. 11. Fig. 11a–c show that the Al atom can not be detected in region I because this region was fully covered by relatively thick nylon film. On the edge of region I, the nylon was tore away from the AA6061 under the high tensile stress and a low density of Al atom was found. The density of Al atoms increased and the density of C atoms decreased obviously from region I to III, indicating a significant decrease in the thickness of the nylon from region I to III. It should be noted that although the residual nylon was hardly observed directly by SEM in region III (Fig. 10c), the SEM–EDS mapping showed that the sparse C atoms was coexistent with C rich spots in this region. The position of the C rich spots corresponded well with the Al lacking spots in region III. This indicated that a weak chemical interaction between AA6061 and MC Nylon occurred in region III.

The contrast of regions II and III is shown in Fig. 11d–f. Region III was characterized by sparse C atoms coexisting with a small number of C rich spots while large numbers of C rich (Al lacking) zones were observed in region II. This is because region II was covered by much more nylon compared with region III. Region IV was covered by sparse C atoms coexisting with a small number of C rich zones (Fig. 11g–i). The density of C atoms in region IV was in between regions II and III, which was consistent with the observation of the thin and small detrital nylons in region IV (Fig. 10d and h). Fig. 11j–l show that high concentration of C atoms almost without Al atoms were detected in the area which was covered by ridge shaped nylon while both C and Al atoms were detected on both sides of this area. This indicated that the thickness of the ridge shaped nylon is much thicker than that of the residual nylon around.

To understand the generation of the ridge shaped nylon in regions V, VI and VII, the typical fracture surface of the sample 2000–800 was subjected to SEM examination further. Fig. 12a shows that many ridge shaped nylons were connected to the nylon film in the bubble regions (region I). Fig. 12b shows the typical

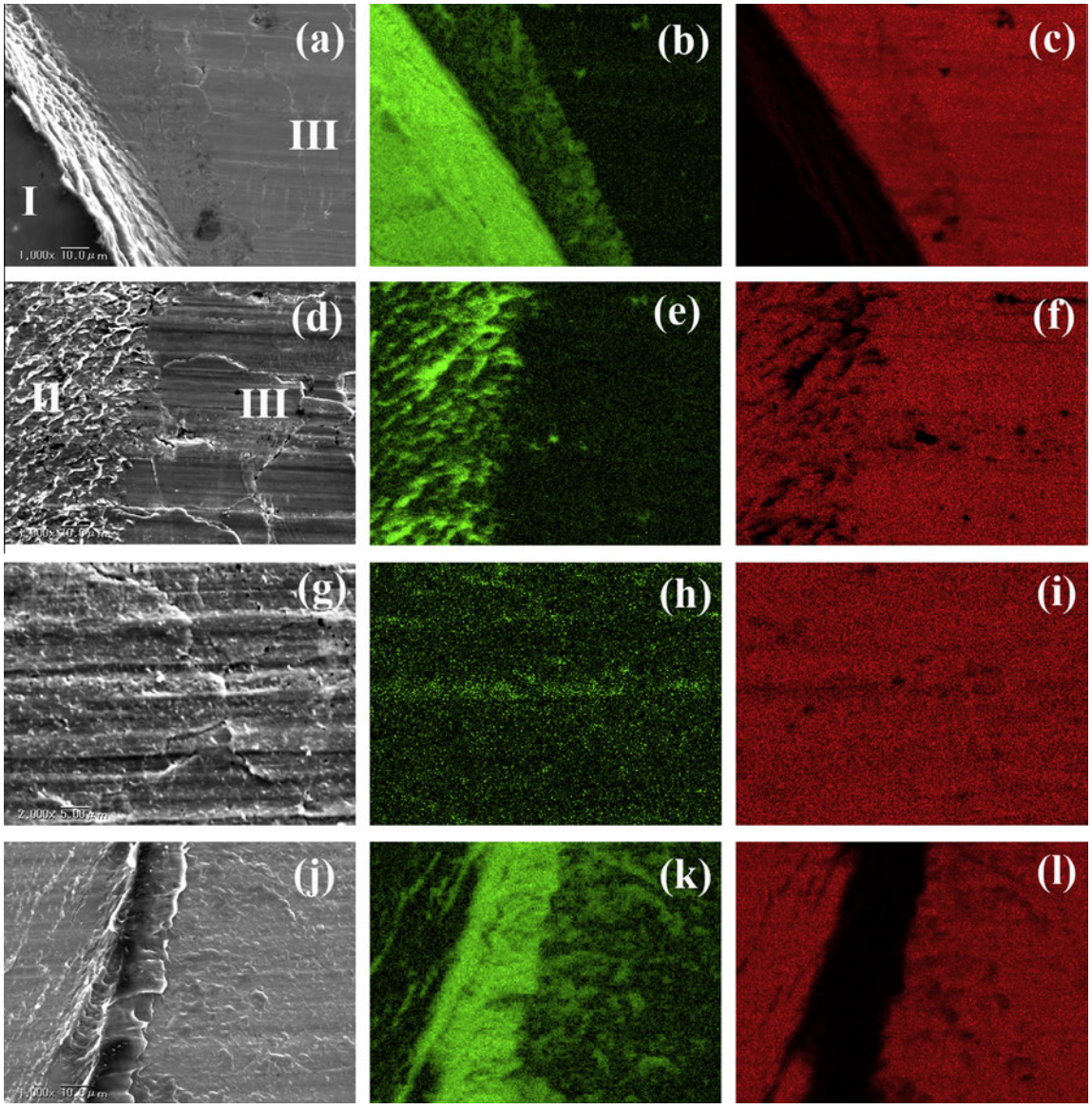

Fig. 11. SEM–EDS results obtained over interface of regions I and III for (a) high magnification, (b) C and (c) Al distribution; over interface of regions II and III for (d) high magnification, (e) C and (f) Al distribution; in region IV for (g) high magnification, (h) C and (i) Al distribution; and in region V for (j) high magnification, (k) C and (l) Al distribution.

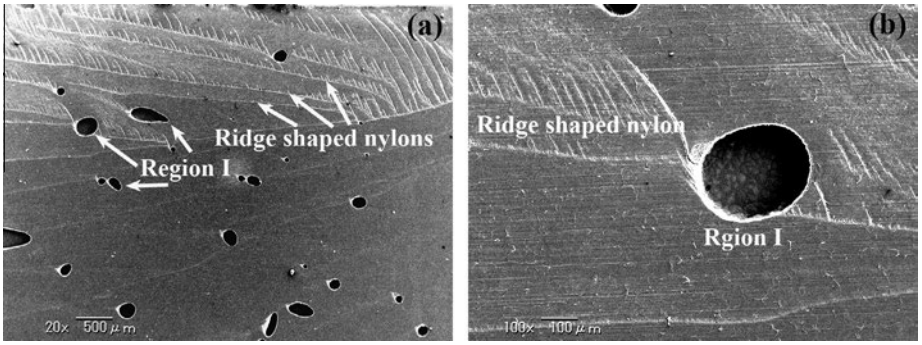

Fig. 12. Typical SEM images obtained from fracture surface of sample 2000–800: (a) low magnification and (b) high magnification.

Table 3
Ratio of various regions to fracture surface for sample processed at different FLW parameters.

Sample	Region I (%)	Region II (%)	Region III (%)	Region IV (%)	Region V (%)	Region VI (%)	Region VII (%)	NSS (MPa)
1000–200	45	13	42	–	–	–	–	5.1
1000–400	9	18	57	16	–	–	–	7.5
1000–800	6	–	43	38	13	–	–	5.3
2000–200	33	21	46	–	–	–	–	7.5
2000–400	8	–	20	30	42	–	–	7.6
2000–800	5	–	14	71	–	10	–	6.9
2000–1500	2	–	36	41	–	–	21	4.8
3000–200	19	27	54	–	–	–	–	8.1
3000–400	4	12	52	10	22	–	–	7.7
3000–800	2	–	17	37	–	44	–	7.6
3000–1500	1	–	19	66	–	–	14	5.0

development of ridge shaped nylons from the edge of region I. The bubbles generated during FLW provided high pressure and simultaneously pushed the molten nylon onto the AA6061 surface. The nylon film in region I endured higher pressure than the nylon around during FLW and was tightly bonded to the AA6061 surface. Therefore, the interface between the nylon in regions I and AA6061 is supposed to have the ability to bear higher tensile stress. It is hard to tear this nylon film off AA6061 during the tensile test, resulting in stress concentration at the edges of region I. The stress concentration was relieved by the rapid crack propagation in the nylon when the stress reached a critical level and the ridge shaped nylon was left on the AA6061 surface. The authors supposed that the stress concentration and crack propagation in the nylon mainly were responsible for the appearance of ridge shaped nylon.

4.5. Influence of fracture morphology on NSS

The analyses above indicated that the contribution of the region I to the shear strength should be very limited because the nylon film in the region I was tore off only along the narrow edges. The contribution of region III to the shear strength was also low because the interfacial chemical interaction between AA6061 and nylon was weak in this region. Therefore, the shear strength of the sample 2000–200 was mainly provided by region II (Fig. 9a). An increase in the proportion of region II in the hybrid lap joint would be beneficial to increase the shear strength. This was confirmed by the statistics summarized in Table 3. The NSS increased with increasing the area of regions II for the hybrid lap joints produced at a welding speed of 200 mm/min and various rotation rates (Table 3). The sample 3000–200 which contained about 27% region II exhibited the highest NSS, showing the high shear stress bearing ability of region II.

The shear load of the samples 1000–800, 2000–800, 2000–1500 and 3000–1500, was mainly undertook by region IV (Table 3). These samples exhibited low NSS even though high ratio of region IV was observed on the fracture surface, indicating that region IV is weak in shear stress bearing ability. Both the sample 2000–400 which contained 42% region V and the sample 3000–800 which contained 44% region VI exhibited a high NSS of 7.6 MPa. A comparison between the samples 2000–400 and 2000–800 showed that the NSS increased with an increase in the ratio of region V and a decrease in the ratio of region IV. Similarly, samples 3000–800 and 3000–1500 showed that increasing the ratio of region VI along with decreasing the ratio of region IV was beneficial to the NSS improvement. This indicated that the regions which contained ridge shaped nylon could endure higher shear stress compared with region IV which was covered by thin and small detrital nylons. Based on the above analyses, the shear strength bearing ability of these regions should follows such an order: region II > region V > region VI > region VII > region IV > region I or III. Increasing the area fraction of the region II in the hybrid joints is our efforts in the future.

4.6. Main advantages of FLW

FLW can be performed using the existing FSW machines, modified machine tools or purpose-designed equipment. This makes the FLW process suitable for automation and robot use, and thereby enhances its design flexibility and industrial application. Other important benefits of the process are as follows. (i) High quality joining can be obtained under a suitable FLW design. This study showed that the highest NSS of the hybrid AA6061 and MC Nylon-6 joint reached as high as about 8 MPa even without any surface preparation. Because FLW is conducted below the melting temperature of the jointed metal, the alloying loss, mechanical property reduction and workpeice distortion in the metal are less. Distortion in the MC Nylon-6 can also be avoided under proper FLW parameters and fixture. (ii) FLW is an efficient welding method. FLW can be achieved at high welding speeds and significantly fewer parameters (only four variables: tool dimension, rotation rate, weld speed and plunge depth) have to be controlled. (iii) FLW is an energy saving and environmental friendly process. It

does not involve shielding gas, spark showers, noise, glare or electromagnetic hazard during FLW process.

5. Conclusions

The lap joints between MC Nylon-6 and AA6061 aluminium alloy were fabricated by a novel friction lap welding (FLW) technique. Tensile shear test showed that the tool rotation rate and welding speed had great influences on the bond strength. The cross section of the lap joints and the surface morphologies of the fractured tensile samples were investigated. The results can be summarized as follows.

(1) High quality lap joints with the NSS of 5–8 MPa were obtained over a wide range of welding parameters.
(2) A linear relationship was observed between FLW parameters (R^2/v and the thickness of melted nylon (H), where R (rpm) is the rotation rate, and v (mm/min) is the welding speed.
(3) An increase in the FLW rotation rate not only increased the thermal input but also bended the AA6061 plates increasingly toward MC Nylon-6, resulting in a decrese in the volume of bubbles and an enhancement in the NSS of the joints.
(4) Increasing the FLW welding speed reduced both the thermal input and the volume of bubbles.
(5) Residual nylon was observed on the fracture surface of AA6061 plates. SEM–EDS analysis showed that the thickness of nylon left on aluminium surface varied in different regions.
(6) The morphology of the fracture surfaces of AA6061 plates fell into seven types based on the nylon distribution. Statistical analysis showed that the shear strength bearing ability of these regions should follows such an order: region II > region V > region VI > region VII > region IV > region I or III.

Acknowledgment

This work was partly supported by Grant-in-Aid for Scientific Research (A) (No.21246111) from Japan Society for Promotion of Science.

References

[1] Katayama S, Kawahito Y. Laser direct joining of metal and plastic. Scripta Mater 2008;59:1247–50.
[2] Messler RW. Joining composite materials and structure: some thought-provoking possibilities. J Thermalplast Compos 2004;17:51–75.
[3] Amancio-Filho ST, dos Santos JF. Joining of polymers and polymers–metal hybrid structures: recent developments and trends. Polym Eng Sci 2009;49:1416–76.
[4] Fink A, Camanho PP, Andres JM, Pfeiffer E, Obst A. Hybrid CFRP/titanium bolted joints: performance assessment and application to a spacecraft payload adaptor. Compos Sci Technol 2010;70:305–17.
[5] Wahba M, Kawahito Y, Katayama S. Laser direct joining of AZ91D thixomolded Mg alloy and amorphous polyethylene terephthalate. J Mater Proc Technol 2011;211:1166–74.
[6] Jung KW, Kawahito Y, Takahashi M, Katayama S. Laser direct joining of carbon fiber reinforced plastic to zinc-coated steel. Mater Des 2013;47:179–88.
[7] Holtkamp J, Roesner A, Gillner A. Advances in hybrid laser joining. Int J Adv Manuf Technol 2010;47:923–30.
[8] Fortunato A, Cuccolini G, Ascari A, Orazi L, Campana G, Tani G. Hybrid metal–plastic joining by means of laser. Int J Mater Form 2010;3:1131–4.
[9] Wang X, Li P, Xu ZK, Song XH, Liu HX. Laser transmission joint between PET and titanium for biomedical application. J Mater Proc Technol 2010;210:1767–71.
[10] Yusof F, Yukio M, Yoshiharu M, Shukor MHA. Effect of anodizing on plused Nd: YAG laser joining of polyethylene terephthalate and aluminium alloy (A5052). Mater Des 2012;37:410–5.
[11] Balle F, Wagner C, Eifler D. Ultrasonic spot welding of aluminium sheet/carbon fiber reinforeced polymer joints. Mat Werkstoff 2007;38:934–8.
[12] Balle F, Wagner C, Eifler D. Ultrasonic metal welding of aluminium sheets to carbon fibre reinforced thermoplastic composites. Adv Eng Mater 2009;11:35–9.
[13] Balle F, Eifler D. Statistical test planning for ultrasonic welding of dissimilar materials using the example of aluminium carbon fiber reinforced polymers (CFRP) joints. Mat Werkstoff 2012;43:286–92.
[14] Filho STA, Bueno C, Sabtos JF, Huber N, Hage E. On the feasibility of friction spot joining in magnesium/fiber reinforced polymer composite hybrid structures. Mater Sci Eng A 2011;528. 384-48.
[15] Yusof F, Miyashita Y, Seo N, Mutoh Y, Moshwan R. Utilising friction spot joining for dissimilar joint between aluminium alloy (A5052) and polyethylene terephthalate. Sci Tech weld join 2012;17:544–9.
[16] Nakata K. International Patent Application No. PCT/JP2012/053839.
[17] Mishra RS, Ma ZY. Friction stir welding and processing. Mater Sci Eng R 2005;50:1–78.
[18] Liu FC, Ma ZY. Influence of tool dimension and welding parameters on microstructure and mechanical properties of friction-stir-welded 6061–T651 aluminum alloy. Metall Mater Trans A 2008;39:2378–88.
[19] Cui GR, Ma ZY, Li SX. Periodical plastic flow pattern in friction stir processed Al–Mg alloy. Scripta Mater 2008;58:1082–5.
[20] Bhardwaj IS, Kumar V, Mathur AB, Das A. Characterization of multiphase polymer system MC nylon/ABS blends. J Therm Anal 1990;36:2339–47.
[21] Braun E, Levin BC. Nylons: a review of the literature on products of combustion and toxicity. Fire Mater 1986;11:71–88.
[22] Tang W, Guo X, McClure JC, Murr LE. Heat input and temperature distribution in friction stir welding. J Mater Process Manufact. Sci 1998;7:163–72.
[23] Colegrove PA, Shercliff HR. Development of Trivex friction stir welding tool Part 1 Two-dimensional flow modelling and experimental validation. Sci Technol Weld Join 2004;9:345–51.
[24] Arbegast WJ, Hartley PJ. Friction stir weld technology development at lockheed martin michoud space systems – an overview. In: Proc 5th int conf trends welding res, June 1–5. Pine Mountain, GA; 1998. p. 541–6.
[25] Ren SR, Ma ZY, Chen LQ. Effect of welding parameters on tensile properties and fracture behaviour of friction stir welded Al–Mg–Si alloy. Scripta Mater 2007;56:69–72.